IPC

Indonesian Physics Communication

Department of Physics, Universitas Riau, Pekanbaru, Indonesia
p-ISSN 1412-2960 | e-ISSN 2579-521X

Vol. 22 | No. 2
July 2025

Web: https://kfi.ejournal.unri.ac.id
E-mail: kfi@ejournal.unri.ac.id

The effect of copper doping on the structural properties and composition of iron oxide nanoparticles of Ulakan Pariaman Beach sand prepared by the ball milling method

Diny Fandriani, Erwin*
Department of Physics, Universitas Riau, Pekanbaru 28293, Indonesia

*Corresponding author: erwin.amiruddin@lecturer.unri.ac.id

ABSTRACT

This study explores the utilization of beach sand from Ulakan Pariaman as a source of iron oxide-based magnetic material through processes of separation, refinement, and copper (Cu) doping. The samples were processed using an iron sand separator (ISS) to separate iron oxide from other oxides, followed by treatment with a neodymium iron boron (NdFeB) magnet and ball milling technique with variations in milling time and ball size Cu doping was applied to compositions of $(Fe_2O_3)_{100-x}Cu_x$ where x = 0; 5; 10; 15; and 20 wt.%, to investigate changes in structural and magnetic properties. XRD characterization revealed the dominance of the spinel phase of magnetite (Fe_3O_4) and a partial transformation to maghemite (γ-Fe_2O_3) indicated by changes in peak width and intensity. XRF analysis confirmed a decrease in Fe content and an increase in Cu concentration, suggesting ionic substitution within the crystal lattice. Magnetic susceptibility with higher increasing Cu content, demonstrating a positive effect of doping on the material's magnetic response.

Keywords: Ball milling; copper dopping; iron oxide nanoparticles; magnetic susceptibility; natural sand

Received 22-05-2025 | Revised 06-06-2025 | Accepted 13-06-2025 | Published 31-07-2025

INTRODUCTION

Indonesia is a country rich in natural resources, including iron oxide minerals, which are found abundantly along the coast. Iron sand is a source of iron oxide minerals that holds significant potential in various technological applications, such as the steel industry, magnetic materials, and functional nanomaterials [1]. One area with iron sand resources is Ulakan Beach, Pariaman, West Sumatra, which has not been optimally utilized in the development of advanced nanotechnology-based materials.

Nanotechnology utilizes atoms and molecules on a much smaller scale, around 100 nanometers. One example of a highly developed nanomaterial is Fe_3O_4 nanoparticles. Iron sand has potential as a source of nanoparticles because it contains magnetic minerals such as magnetite (Fe_3O_4), hematite (α-Fe_2O_3), and maghemite (γ-Fe_2O_3). To create Fe_3O_4 nanoparticles with a homogeneous and fine grain size, several synthetic methods are used, such as coprecipitation, sol-gel, solid-state, hydrothermal, molten salts, and others [2-4]. However, to improve the performance of this material, modification is required through doping techniques with other elements, such as copper (Cu) to optimize its structural and magnetic properties.

Transition metal element doping has been widely used to improve the magnetic and electrical properties of iron oxide-based materials. Copper (Cu) is a dopant that can affect the structural and magnetic properties of iron oxide by replacing some of the Fe3+ ions in the crystal lattice, thus causing changes in the lattice parameters and crystal structure of the material [5]. According to research conducted by Chaudari (2024) [6], Cu doping in Fe_2O_3 can cause a phase change from hematite (α- Fe_2O_3) to maghemite (γ-Fe_2O_3) with a cubic crystal structure that has better ferromagnetic

properties than hematite. This phenomenon occurs due to the difference in ionic radii between Cu^{2+} (0.73 Å) and Fe^{3+} (0.64 Å), which causes lattice distortion and a decrease in crystal size [7].

In this study, copper (Cu) doping was carried out on iron oxide nanoparticles originating from Ulakan Pariaman beach sand to understand how the crystal structure and magnetic properties change.

RESEARCH METHODS

This study used natural sand from Ulakan Beach in Pariaman, West Sumatra Province. Sampling was conducted at five different locations: A, B, C, D, and E. The sampling method used a grid model at each predetermined location, with a sampling area of 1 meter × 1 meter. The distance between sampling points was set at 200 cm, and four samples were taken at each location, each weighing 1 kg, resulting in a total sample collection of 20 kg from the five locations. The natural sand samples were dried under sunlight to remove water content, facilitating the separation of magnetic and non-magnetic particles. After the samples dried, they were separated using an iron sand separator (ISS). This process separates the magnetic and non-magnetic particles. Before the samples were processed on the ISS, they were weighed to determine their mass.

The working principle is that the dried sample is slowly inserted into a vibrator that flows to a conveyor which is then carried by a belt to an electromagnetic wheel which is where the magnetic and non-magnetic particles are separated. Then the concentrate container is filled with samples containing magnetic particles while samples that do not contain magnetic particles will enter the sand container. Samples that have gone through the separation of magnetic and non-magnetic particles are the products of the ISS crushed using a BM tool for 3 hours using 18 iron balls with a diameter of 1.5 cm. This BM process aims to produce a smoother product. Samples that have gone through this process are then separated using Neodymium Iron Boron (NdFeb) magnets. This process is called the first stage of BM (Product BM1). Next, repeat the steps that have been done for the BM1 product, but with an extended time of 15 hours and using the same number and diameter of balls. Then, perform the third step, repeating steps 1 and 2 using 50 0.5 cm diameter iron balls and 18 1.5 cm diameter balls for 102 hours. Thus, the total time spent during the ball milling process is 120 hours, resulting in a very fine concentrate.

The results of this 120-hour ball milling process are separated into five parts: BM3A, BM3B, BM3C, BM3D, and BM3E. Each BM3A, BM3B, BM3C, BM3D, and BM3E product is doped with copper at varying weight percentages (%wt). BM3A was not doped 0%wt, BM3B was doped at 5%wt (0.95 grams of sample and 0.05 grams of copper), BM3C was doped at 10%wt (0.9 grams of sample and 0.1 grams of copper), BM3D was doped at 15%wt (0.85 grams of sample and 0.15 grams of copper), and BM3E was doped at 20%wt (0.8 grams of sample and 0.2 grams of copper). Furthermore, the BM3B, BM3C, BM3D, and BM3E products were Ball Milled for 20 hours, resulting in nanoparticles called BM4A, BM4B, BM4C, BM4D, and BM4E. The BM4 product was divided into three parts: BM4A with a weight percentage of 0 wt%, BM4B with a weight percentage of 5 wt%, and BM4C with a weight percentage of 10 wt%. Each product was then placed in a glass bottle for testing using a Vibrating Sample Magnetometer (VSM) and a Scanning Electron Microscope (SEM).

The coreless magnetic induction measurement used a Pasco PS-2162 probe sensor and a solenoid with 2,500 turns, measuring 3 cm in diameter and 10 cm in length. The Pasco PS-2162 probe sensor was connected to a laptop with Data Studio software installed. The coreless solenoid B0 magnetic induction measurement was performed by setting a fixed distance of 1 mm from the sensor. The Pasco PS-2162 probe was energized without inserting a sample into the

solenoid, with currents of 0.1 A, 0.2 A, 0.4 A, 0.6 A, and 0.8 Amperes. The magnetic susceptibility value is calculated by dividing the total magnetic induction (B_T) by the magnetic induction of the solenoid without a core (B_0), then dividing by the magnetic induction of the solenoid without a core (B_0).

Next, the crystallinity properties were analyzed using the X-Ray Diffraction (XRD) method on several samples, including BM4 products such as BM4A (0 wt% Cu), BM4B (5 wt% Cu), and BM4C (10 wt% Cu). Composition testing using X-Ray Fluorescence (XRF) on Ulakan natural sand and ball milled products was conducted using several BM4 product samples, namely BM4A (0 wt% Cu) and BM4B (5 wt% Cu).

RESULTS AND DISCUSSION

Solenoid Magnetic Induction Measurement

The solenoid magnetic induction was measured using a Pasco PS-2162 Probe magnetic sensor connected to a laptop with a cylindrical solenoid measuring 10 cm long (L), 3 cm in diameter (D), and 2,500 turns (N). The solenoid core measured was Ulakan Pariaman beach sand, which had been ball milled for 120 hours. The BM4 product, doped with copper (Cu), was used. The magnetic induction measurement data for the coreless solenoid (B0) with a fixed spacing of 1 mm as a function of current is shown in Figure 1.

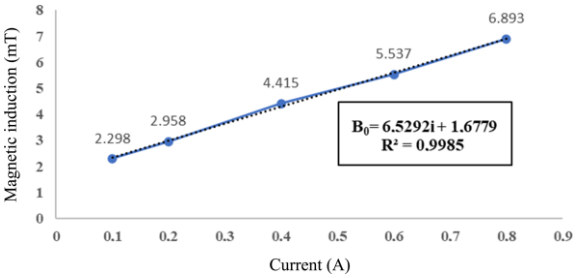

Figure 1. Graph of the coreless magnetic induction as a function of current with a fixed spacing of 1 mm.

Figure 1 shows that the magnetic induction in the solenoid increases linearly with increasing current. Based on the measurement results, the magnetic induction value at a current of 0.1 A was 2.298 mT, increasing to 6.893 mT when the current reached 0.8 A. This relationship can be represented by the linear regression equation $B_0 = 6.5292i + 1.6779$ with $R^2 = 0.9985$. When I = 0 mA, B_0 will be 1.6779 mT, indicating a very strong relationship between current and magnetic induction and following a linear pattern with a high degree of accuracy.

This is consistent with the basic concept of the magnetic field in a solenoid: magnetic induction is proportional to the flowing electric current. This increase in magnetic induction occurs because the greater the current passing through the solenoid coil, the stronger the magnetic field generated within it. This increase is consistent with the theory of magnetic induction in solenoids: if the current is increased, the magnetic induction value in each sample will increase linearly. This phenomenon has been extensively studied in modern electromagnetism studies, where various magnetic field-based applications, such as magnetic sensors and data storage devices, rely heavily on the linear relationship between magnetic induction and electric current [5].

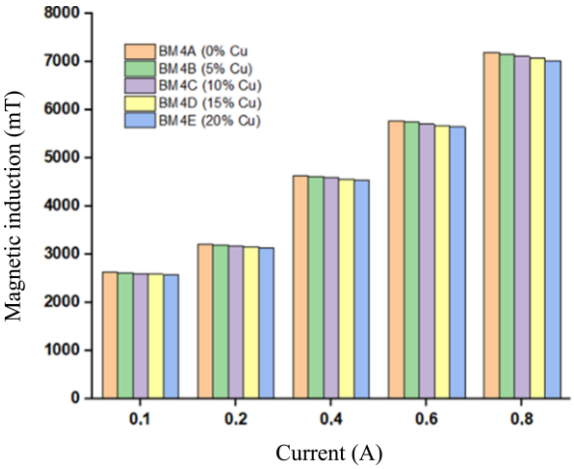

Figure 2. Magnetic induction of a solenoid with varying current and copper (Cu) doping.

Figure 2 shows the results of magnetic induction measurements of a solenoid with varying current. The magnetic induction value increases with increasing applied electric

current. It can be observed that at a current of 0.1 A, the magnetic induction value ranges from 2.583 mT to 2.633 mT, while at a current of 0.8 A, the magnetic induction value increases to approximately 7.032 mT to 7.196 mT. This increase is consistent with the magnetic field theory in solenoids, which states that the generated magnetic field is directly proportional to the applied electric current.

The effect of copper (Cu) doping on magnetic induction of the undoped Cu sample (BM4A) has the highest magnetic induction value compared to samples doped with Cu at various concentrations. In BM4A (0% Cu) with a current of 0.8 A, the magnetic induction reached 7.196 mT, while in BM4E (20% Cu), the value decreased to 7.032 mT. This decrease indicates that the addition of Cu to the Fe_2O_3 material reduces its magnetic properties. This is due to the diamagnetic nature of Cu^{2+}, which disrupts the spin interactions between the Fe^{2+} and Fe^{3+} ions in Fe_2O_3, thereby reducing the total magnetization. On an atomic scale, Cu^{2+} ions replace Fe ions in the Fe_2O_3 crystal lattice, disrupting the electron spin interactions that contribute to the material's magnetic properties.

Magnetic Susceptibility

Figure 3 show data and a graph of magnetic susceptibility values for Cu-doped copper with a current of 0.8 A, varied using Cu at different concentrations (wt.%): 0 wt.%; 5 wt.%; 10 wt.%; 15 wt.%; and 20 wt.% were ball milled for 20 hours. The magnetic susceptibility values of each sample were 4395.76×10^{-5}; 3760.08×10^{-5}; 3211.29×10^{-5}; 2617.33×10^{-5}; and 2018.87×10^{-5}. The susceptibility value for Cu doping results decreased with increasing concentration. This decrease is due to the basic nature of Cu which is a diamagnetic material. Diamagnetism in Cu arises because all of its electron orbitals are fully filled, so it does not have an intrinsic magnetic moment. When diamagnetic Cu^{2+} ions replace some of the paramagnetic Fe^{3+} ions in the Fe_2O_3 lattice, the contribution to the total magnetic moment decreases. Furthermore, the presence of Cu^{2+} ions also disrupts the spin regularity in the lattice, which further weakens the magnetic interactions between Fe^{3+} ions. Therefore, the higher the Cu doping concentration added, the lower the magnetic susceptibility value.

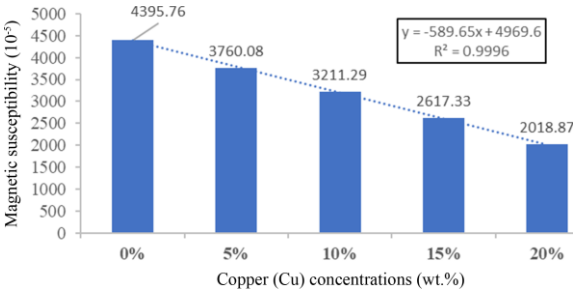

Figure 3. Graph of magnetic susceptibility values for Cu-doped copper (Cu) with a current of 800 mA.

X-Ray Diffraction (XRD) Results

Figure 4 shows the X-ray diffraction results of a BM4A sample (0 wt.% Cu), which exhibits a diffraction pattern typical of the magnetite phase (Fe_3O_4) with a cubic spinel structure. The main diffraction peaks appear at 2θ angles of approximately 28.12°, 30.12°, 33.2°, 35.36°, 43.43°, 53.19°, 56.51°, and 62.34°, which correspond to the crystal planes (012), (220), (104), (311), (400), (422), (511), and (440).

The highest peak is at an angle of 35.36° with a Miller index of (311), which is a significant peak of the main phase formed, the magnetite Fe3O4 phase. Based on calculations using the Scherrer equation, the average crystallite size for the BM4A sample is 28.93 nm with a smaller FWHM value than the other samples, namely 0.3071°. This indicates that BM4A still has high crystallinity with minimal disruption in its crystal lattice structure.

Figure 5 shows the X-ray diffraction pattern after doping with 5 wt.% Cu. There is a change in the intensity of the diffraction peaks. The main diffraction peaks appear at 2θ angles of approximately 29.82°, 35.38°, 43.58°, 53.56°, 56.68°, and 62.49°, which correspond to the (220), (311), (400), (422), (511), and (440) crystal planes, which are typical of the spinel magnetite (Fe_3O_4) structure. Several major peaks, such as (220), (311), (400), and (511),

exhibit a slight shift toward larger angles and a decrease in intensity, indicating lattice distortion due to partial substitution of Fe^{2+} ions by Cu^{2+} ions.

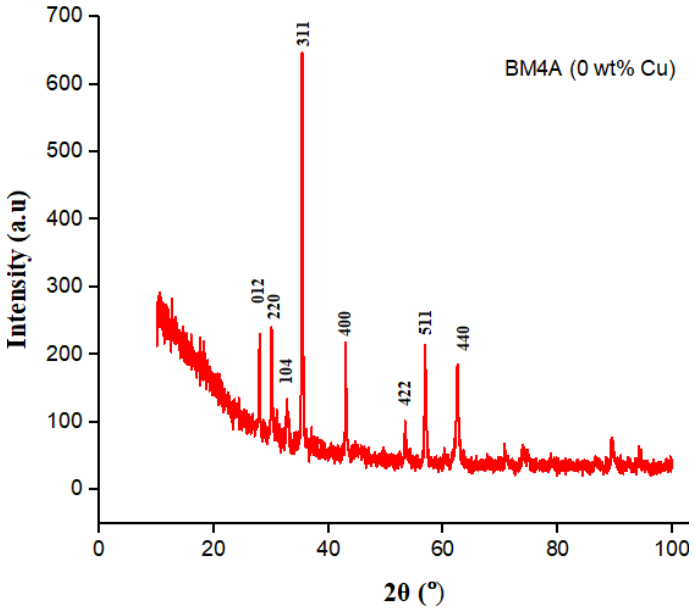

Figure 4. X-ray diffraction pattern of a BM4A sample doped with 0 wt.% Cu.

Cu doping of 5 wt.% causes an increase in the Full Width at Half Maximum (FWHM) value to 0.3365°, which contributes to a decrease in the crystallite size to 24.81 nm. This indicates that Cu doping disrupts the crystal regularity (decreased crystallinity) and amplifies the lattice distortion effect. The primary phase remains the spinel magnetite (Fe_3O_4) structure, rather than hematite (α-Fe_2O_3), as supported by the position and pattern of the diffraction peaks. This is consistent with research conducted by Kołodziej (2023) [8], which states that doping transition metal ions into iron oxide can cause changes in lattice parameters, a decrease in crystallite size, and a decrease in crystallinity due to ion size mismatch.

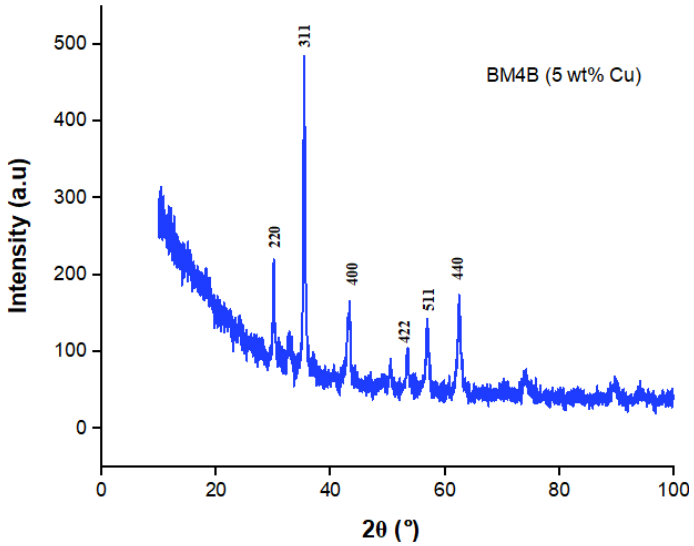

Figure 5. X-ray diffraction pattern of a BM4B sample doped with 5 wt.% Cu.

Figure 6 shows the X-ray diffraction pattern of a BM4C sample (10 wt.% Cu). The main diffraction peaks appear at 2θ angles around 30.18°, 35.42°, 43.03°, 50.78°, 53.64°, 57.25°,

and 62.74°, which correspond to the (220), (311), (400), (422), (024), (511), and (440) crystal planes, respectively, which are the reference for the $CuFe_2O_4$ spinel phase. Additionally, there are additional minor peaks around 28.10° and 32.91°, which likely indicate the emergence of minor phases such as CuO or other mixed oxides due to increased Cu doping.

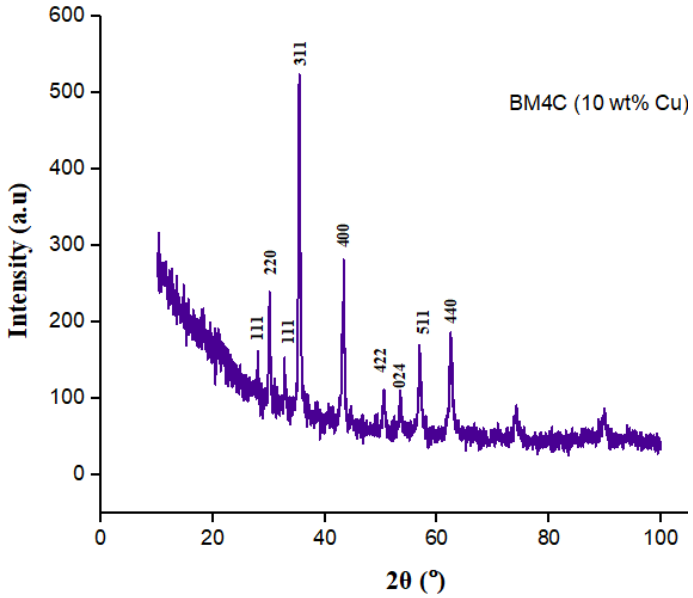

Figure 6. X-ray diffraction pattern of a BM4C sample doped with 10 wt.% Cu.

The main peaks, such as (311) and (400), shift further toward larger 2θ angles, indicating lattice distortion due to increased substitution of Cu^{2+} ions into Fe^{2+} ion positions in the spinel structure. The crystallite size of the BM4C sample decreased to 23.93 nm with a larger FWHM (0.3490°) than the BM4A and BM4B samples. The increased FWHM indicates greater imperfections in the crystal structure. The decreased crystallite size indicates decreased crystallinity due to doping. The main phase in the BM4C sample is dominated by the spinel structure (Fe_3O_4 and/or $CuFe_2O_4$).

However, the increased peak width and decreased intensity of the main peak may indicate a possible partial transformation of the structure to maghemite (γ-Fe_2O_3), which has a cubic spinel structure with high lattice defects and a diffraction pattern very similar to magnetite.

Table 1. Strongest diffraction peaks (strongest lines) for each sample.

Cu doping (wt.%)	hkl	Angle 2θ (°)	FWHM (°)	Crystalline size (nm)
0 (BM4A)	(311)	35.36	0.3071	28.93
5 (BM4B)	(311)	35.38	0.3365	24.81
10 (BM4C)	(311)	35.42	0.3490	23.93

Table 1 shows that increasing the Cu concentration increases the FWHM (Full Width at Half Maximum). The higher the FWHM, the smaller the crystallite size, and vice versa. Samples BM4A, BM4B, and BM4C have average crystallite sizes of 28.93 nm, 26.44 nm, and 25.51 nm, respectively. The smaller atomic size of Cu compared to Fe results in a decrease in crystallite size and an increase in the diffraction angle at 2θ, approximately 35°.

X-Ray Fluorescence (XRF) Results

According to Figure 7, the data obtained show that magnetic elements include Al (Aluminum), Ti (Titanium), Mn (Manganese), Fe (Iron), and Ni (Nickel). Meanwhile, non-

magnetic elements include Si (Silicon), P (Phosphorus), Ca (Calcium), S (Sulfur), Ag (Silver), and Cu (Copper). Before Cu doping, the Fe content in the sample was 74.88%. However, after doping with 5 wt.% Cu, the Fe content decreased to 69.41%, indicating that some Fe ions had been replaced by Cu in the crystal structure. Conversely, the Cu concentration increased drastically from 0.017% to 13.161%, indicating the success of the Cu doping process in the material.

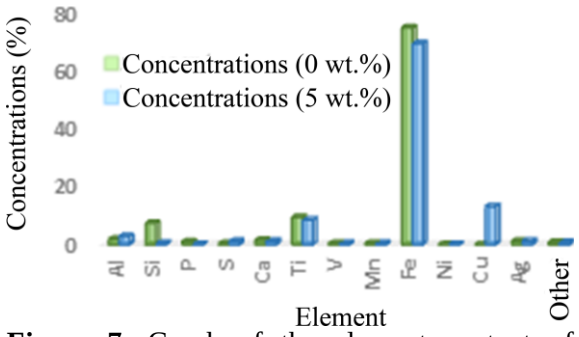

Figure 7. Graph of the element content of Ulakan Pariaman beach sand after 120 hours of multi-step ball milling and 20 hours of ball milling with copper (Cu) doping.

In addition to Fe and Cu, several other elements also experienced changes in concentration after the ball milling and doping processes. The Si content decreased drastically from 7.357% to 0.43%, indicating that most of the silicate compounds were eliminated during the milling process. Other elements, such as Al and Ni, experienced small increases, while elements such as Ti, Mn, and V experienced slight decreases. These changes can occur due to mechanochemical effects during the milling process, which cause redistribution of elements within the material and changes in its microstructure. These changes in elemental composition are also influenced by the duration of the ball milling process, which affects particle size and element distribution within the material.

CONCLUSION

The susceptibility value for Cu doping results increases with increasing concentration. The XRD characterization results show that the beach sand particles processed using ball milling have a magnetite phase (Fe_3O_4) with a cubic spinel structure, and the BM4C sample remains dominated by the spinel structure (Fe_3O_4 and/or $CuFe_2O_4$). However, the increase in peak width and decrease in the intensity of the main peak may indicate the possibility of partial transformation of the structure into maghemite (γ-Fe_2O_3), which has a cubic spinel structure with high lattice defects and a diffraction pattern very similar to magnetite. The addition of Cu doping causes a decrease in crystallite size with sizes for BM4A, BM4B and BM4C samples of 28.93 nm, 24.81 nm and 23.93 nm, respectively. The results of X-Ray Fluorescence (XRF) identification indicate that the beach sand processed using ball milling contains various elements, both magnetic and non-magnetic. Elements included in the magnetic group include Al, Ti, Mn, Fe, and Cu, while non-magnetic elements include Si, P, Ca, Ag, and other elements.

REFERENCES

1. Budiman, A. (2014). Pemetaan Persentase Kandungan Dan Nilai Suseptibilitas Mineral Magnetik Pasir Besi Pantai Sunur Kabupaten Padang Pariaman Sumatera Barat. *Jurnal Fisika Unand*, **3**(4), 242–248.
2. Oktaviani, E., Nasri, M. Z., & Deswardani, F. (2020). Sintesis dan karakterisasi nanopartikel Fe_3O_4 (Magnetite) dari pasir besi sungai Batanghari Jambi yang dienkapsulasi dengan polyethylene glycol (Peg-4000). *Jurnal Pendidikan Fisika Tadulako Online*, **8**(3), 97–103.
3. Erwin, E. & Putra, S. U. (2018). Sifat Magnetik Dan Ukuran Partikel Magnetik Serta Komposisi Material Pasir Besi Pantai Kata Pariaman Sumatera Barat Di Sintesa Dengan Iron Sand Separator Dan Ball Milling. *Journal Online of Physics*, **3**(2), 11–14.
4. Amiruddin, E., Awaluddin, A., Sihombing, M., Royka, A., & Syahrul, T. (2020).

Morphology and structural properties of undoped and cobalt doped magnetic iron oxide particles for improving the environmental quality. *International Journal of Engineering and Advanced Technology (IJEAT)*, **9**(6), 2249–8958.

5. Lassoued, A., Lassoued, M. S., Dkhil, B., Gadri, A., & Ammar, S. (2017). Structural, optical and morphological characterization of Cu-doped α-Fe2O3 nanoparticles synthesized through co-precipitation technique. *Journal of Molecular Structure*, **1148**, 276–281.
6. Chaudhari, D. S., Upadhyay, R. P., Shinde, G. Y., Gawande, M. B., Filip, J., Varma, R. S., & Zbořil, R. (2024). A review on sustainable iron oxide nanoparticles: syntheses and applications in organic catalysis and environmental remediation. *Green Chemistry*, **26**(13), 7579–7655.
7. Griffiths, D. J. (2023). *Introduction to electrodynamics*. Cambridge University.
8. Kołodziej, T., Piętosa, J., Puźniak, R., Wiśniewski, A., Król, G., Kąkol, Z., Biało, I., Tarnawski, Z., Ślęzak, M., Podgórska, K., Niewolski, J., Gala, M. A., Kozłowski, A., Honig, J. M., & Tabiś, W. (2023). Impact of hydrostatic pressure, nonstoichiometry, and doping on trimeron lattice excitations in magnetite during axis switching. *Physical Review B*, **108**(24), 245148.